Dynamical restrictions to squeezing in a degenerate optical parametric oscillator

Lev I. Plimak and Dan F. Walls
Department of Physics, University of Auckland, Private Bag 92019, Auckland, New Zealand
(Received 19 November 1993)

Dynamical restrictions to the squeezing achievable by means of a degenerate optical parametric oscillator (OPO) are considered by quantum-statistical diagram techniques. We determine optimal pumping conditions which maximize the degree of squeezing in the output signal of the OPO. The maximal spectral squeezing in the OPO's output radiation is found to scale as $N_2^{-\frac{2}{3}}$ where N_2 is the number of photons in the pump mode.

PACS number(s): 42.50.Lc, 05.70.Jk, 05.40.+j

I. INTRODUCTION

In this paper, we present corrections to the linearized approximation to a degenerate optical parametric oscillator (OPO) [1] obtained by quantum-statistical diagram techniques. From the formal viewpoint, the "one-loop" approach to the OPO which we follow was first outlined by Zaidi [2] and used later by Mertens *et al.* [3]. We show how the Dyson equations used in [2,3] may be formulated directly in terms of the linear response functions [4] and time-normal averages [5] characterizing the OPO. Unlike the conventional Dyson equations in Perel-Keldish's techniques [6], the equations found below in this paper have a direct macrosopic interpretation. Not only does this allow us to compute corrections to the linearized approximation to the OPO, but also, and probably even more important, reveals their physical content and thus allows us to define the extent of their consistency and applicability.

We show that the accuracy of the one-loop approximation to the OPO is restricted to a perturbative correction to the linearized approximation. In turn, this simplifies the problem to the extent that an analytical solution becomes possible. This solution reveals completely new physical details of the OPO's behavior close to threshold.

We find that the OPO's quantum properties deteriorate in the threshold region rather than become perfect. The underlying physical mechanism is quite simple. The ideal squeezing in the subharmonic radiation, characteristic of the linearized theory, implies unrestricted growth of the fluctuations in its antisqueezed quadrature. Sufficiently close to the threshold, the presence of this noise (which is in effect classical) becomes essential for the OPO's quantum dynamics and results in a general deterioration of the OPO's quantum properties. The optimal pumping conditions are found exactly where this effect of the critical fluctuations becomes noticeable.

One might expect that this "critical repulsion" mechanism is quite general. The squeezing in one quadrature is inevitably connected with growing fluctuations in another quadrature. Thus the squeezing cannot become ideal because the critical fluctuations would then diverge and destroy the squeezing however small the nonlinearity. The maximum achievable squeezing should be expected at a point where the squeezing and the destroying effect of the fluctuations come to balance. These considerations are likely to be useful for defining the optimal pumping conditions for other nonlinear quantum systems.

II. QUANTUM DYNAMICAL THEORY OF FLUCTUATIONS IN THE OPO

A. Dyson equations for the two-point quantum averages

Consider a degenerate OPO [1], i.e., two coupled modes with the resonance frequencies $2\omega_1 = \omega_2$ and widths γ_1 and γ_2, where indices 1 and 2 correspond to the subharmonic and fundamental, respectively. Their nonlinear interaction is described by the effective Hamiltonian of the form

$$H_{\rm int} = \frac{\kappa}{2} a_1^2 a_2^\dagger + \text{H.c.}, \tag{1}$$

where a_k and $a_k^\dagger$, $k = 1,2$, are the modes' annihilation and creation operators. We assume that the OPO is pumped on the fundamental frequency, so that the steady-state field amplitudes are $\langle \boldsymbol{a}_k(t) \rangle = \alpha_k e^{-i\omega_k t}$ (slanted letters denote the Heisenberg field operators). For simplicity, κ is assumed to be real and positive.

The following c-number approach to this nonlinear optical system will serve as a benchmark in our consideration. Let

$$\delta\alpha_k(t) = (2\pi)^{-1} \int d\Omega\, e^{-i(\Omega+\omega_k)t} \delta\alpha_{\Omega k} \tag{2}$$

($k = 1,2$) be weak probe signals emitted by external sources,

$$\delta\varepsilon_k(t) = (2\pi)^{-1} \int d\Omega\, e^{-i(\Omega+\omega_k)t} \delta\varepsilon_{\Omega k} \tag{3}$$

(i.e., Ω is a detuning). Under the above-mentioned pumping conditions, the dynamical properties of the

OPO are described by the 2×2 matrices of the normal, K_Ω, and anomalous, $\tilde{K}_\Omega$, linear response functions:

$$\delta\alpha_\Omega = K_\Omega \delta\varepsilon_\Omega + \tilde{K}^*_{-\Omega}\delta\varepsilon^*_{-\Omega}. \tag{4}$$

In the absence of the nonlinear medium, i.e., in the empty resonator, $\delta\alpha_\Omega = K^{(0)}_\Omega \delta\varepsilon_\Omega$, where $K^{(0)}_{\Omega lm} = \delta_{lm}K^{(0)}_{\Omega ll} = \delta_{lm}(\Omega + i\gamma_l)^{-1}$ is the diagonal matrix of the modes' free retarded Green's functions. In the presence of the $\chi^{(2)}$ medium,

$$\delta\alpha_\Omega = K^{(0)}_\Omega \left(\delta\varepsilon_\Omega + \delta\varepsilon^{\text{ind}}_\Omega\right), \tag{5}$$

where $\delta\varepsilon^{\text{ind}}_\Omega$ is the induced polarization of the medium. In turn, the induced polarization is expressed over the field by

$$\delta\varepsilon^{\text{ind}}_\Omega = D_\Omega \delta\alpha_\Omega + \tilde{D}^*_{-\Omega}\delta\alpha^*_{-\Omega}, \tag{6}$$

where D_Ω and $\tilde{D}_\Omega$ are the matrices of the normal and anomalous linear dynamical susceptibilities of the $\chi^{(2)}$ medium. This results in the equations

$$K_\Omega = K^{(0)}_\Omega \left(I + D_\Omega K_\Omega + \tilde{D}^*_{-\Omega}\tilde{K}_\Omega\right), \tag{7a}$$

$$\tilde{K}_\Omega = K^{(0)*}_{-\Omega} \left(\tilde{D}_\Omega K_\Omega + D^*_{-\Omega}\tilde{K}_\Omega\right). \tag{7b}$$

Then, the statistical properties of the random electromagnetic field, $\delta\alpha'_\Omega$, emitted by the OPO can be expressed by those of the effective self-noise sources $\delta\varepsilon'_\Omega$ in the medium, e.g.,

$$\left\langle \delta\alpha'_\Omega \delta\alpha'^*_{\Omega'} \right\rangle = \left\langle \left[K_\Omega \delta\varepsilon'_\Omega + \left(\tilde{K}_{-\Omega}\delta\varepsilon'_{-\Omega}\right)^*\right]\left[\left(K_\Omega \delta\varepsilon'_{\Omega'}\right)^* + \tilde{K}_{-\Omega}\delta\varepsilon'_{-\Omega'}\right]\right\rangle, \tag{8a}$$

$$\left\langle \delta\alpha'_\Omega \delta\alpha'_{\Omega'} \right\rangle = \left\langle \left[K_\Omega \delta\varepsilon'_\Omega + \left(\tilde{K}_{-\Omega}\delta\varepsilon'_{-\Omega}\right)^*\right]\left[K_{\Omega'}\delta\varepsilon'_{\Omega'} + \left(\tilde{K}_{-\Omega'}\delta\varepsilon'_{-\Omega'}\right)^*\right]\right\rangle. \tag{8b}$$

We stress that $\delta\varepsilon'$ describes the *self-noise* properties of the OPO, as opposed to the *coherent external* source $\delta\varepsilon$ in the relations relevant to the linear response.

If the OPO's noise radiation was not in a quantum state, one could find q-number quantities characterizing the OPO by simply expressing them in c-number terms: Kubo's fluctuation-dissipation theorem [4] states that

$$-i\hbar^{-1}\theta(t_1 - t_2)\left\langle \left[\boldsymbol{a}_m(t_1), \boldsymbol{a}^\dagger_l(t_2)\right]\right\rangle = e^{-i\omega_m t_1 + i\omega_l t_2}\int \frac{d\Omega}{2\pi} e^{-i\Omega(t_1 - t_2)} K_{\Omega ml}, \tag{9a}$$

$$-i\hbar^{-1}\theta(t_1 - t_2)\left\langle [\boldsymbol{a}_m(t_1), \boldsymbol{a}_l(t_2)]\right\rangle = e^{-i\omega_m t_1 - i\omega_l t_2}\int \frac{d\Omega}{2\pi} e^{-i\Omega(t_1 - t_2)} \tilde{K}_{\Omega ml}, \tag{9b}$$

and the OPO's noise properties could be formally reexpressed in terms of the time-normal averages,

$$\left\langle \boldsymbol{a}^\dagger_m(t_2)\boldsymbol{a}_l(t_1)\right\rangle = e^{-i\omega_m t_1 + i\omega_l t_2}\left\{\alpha^*_m\alpha_l + \int \frac{d\Omega}{2\pi} e^{-i\Omega(t_1 - t_2)} G_{\Omega ml}\right\}, \tag{10a}$$

$$\left\langle T_+ \boldsymbol{a}_m(t_2)\boldsymbol{a}_l(t_1)\right\rangle = e^{-i\omega_m t_1 - i\omega_l t_2}\left\{\alpha_m\alpha_l + \int \frac{d\Omega}{2\pi} e^{-i\Omega(t_1 - t_2)} \tilde{G}_{\Omega ml}\right\}, \tag{10b}$$

so that $\left\langle \delta\alpha'_\Omega \delta\alpha'^*_{\Omega'}\right\rangle = 2\pi\delta(\Omega - \Omega')G_\Omega$ and $\left\langle \delta\alpha'_\Omega \delta\alpha'_{\Omega'}\right\rangle = 2\pi\delta(\Omega + \Omega')\tilde{G}_\Omega$.

Less obvious, relations (7) and (8) hold for the actual quantitities K_Ω, $\tilde{K}_\Omega$, G_Ω, and $\tilde{G}_\Omega$, characterizing the OPO, provided that these quantitities are redefined in q-number terms by (9) and (10). As is shown in the Appendix, with suitably defined susceptibilities and quantum noise sources, relations (7) coincide with the Dyson equations [10] for K_Ω and $\tilde{K}_\Omega$, while (8) are solutions to the Dyson equations for G_Ω and $\tilde{G}_\Omega$ [cf. (A23)–(A27)]. This is the manifestation of the general one-to-one correspondence existing between QED and classical statistical electrodynamics [7]. Its best known example is Glauber's quantum coherence theory [5] which matches the classical theory within formal replacement of the c-number field averages by the respective time-normal q-number averages. Another example is the quantum input-output as formulated by Gardiner and Collett [8] (see also Klyshko [9]) where a classical characterization of a linear system suffices to describe this system in a q-number approach. In general, one should consider the system's statistical response properties to fully match classical and quantum approaches—see the Appendix for technical details. The system's quantum properties are thus connected exclusively with the nonclassical nature of its "noise."

Note that the choice of units in this paper is intended to make these quantum-classical correspondences more explicit. We use the mode operator normalization such that $[a_m, a^\dagger_m] = \hbar$. This corresponds to the mode Hamiltonian of the form $\omega_m a^\dagger_m a_m$, unlike the standard choice $[a_m, a^\dagger_m] = 1$ and $H = \hbar\omega_m a^\dagger_m a_m$. The Hamiltonian (1) is also written without Planck's constant. As a result, $\hbar$ then proves to be eliminated from all the relations and quantities that have a classical interpretation, being naturally retained only in those which are inherently quantum. For instance, the classical mode energy, $\omega_m|\beta_m|^2$

(β_m is the c-number mode amplitude), turns out to be written without Planck's constant, as opposed to the average number of photons in the mode, $\hbar^{-1}|\beta_m|^2$. (When comparing our relations with the literature, it may simply be assumed that $\hbar = 1$.)

All equations used below are derived in the Appendix by expressing the susceptibilities and quantum noise sources as diagram series in terms of the linear response functions and two-point time-normal averages [cf. (A28)]. By retaining only the diagrams with no loops one finds the well-known linearized approximation to the OPO [1]. Adding of the one-loop diagrams results in an approximation equivalent to that used in [2,3]. However, we shall see that for the OPO the accuracy of the one-loop Dyson equations is restricted to the first nonvanishing nonlinear correction to the linearized approximation. This accuracy is not improved by their self-consistent solution.

A word of caution is necessary here. The restrictions to the accuracy of the one-loop approach concern only its applications to the OPO and is not relevant to its other applications, in condensed matter physics, say. The one-loop Dyson equations are a formal way to pick a subset of diagrams. The question is whether this subset expresses a coherent part of the system's physics, so that retaining higher-order diagrams is not invalidated by the fact that some lower-order diagrams are omitted. For the OPO this turns out to be not the case: the "one-loop" Dyson equations result, e.g., in an incomplete set of the two-loop diagrams being chosen as an approximation to the noise source on the subharmonic [cf. (A36)]. What is important is not that some of the two-loop diagrams are omitted, but that *for the OPO* the omitted diagrams cannot be expected to be smaller than the ones retained [cf. the discussion following (A36)]. However, this does not affect their accuracy or inaccuracy in other problems.

For the OPO, the one-loop Dyson equations give good results except in the region near the classical threshold.

B. Linearized theory

In the linearized (loopless) approximation, one can write the closed set of equations describing the linear response near the subharmonic frequency [cf. (A41)],

$$K_{\Omega 11} = K^{(0)}_{\Omega 11}\left(1 + d_\Omega K_{\Omega 11} + \tilde{d}^*_{-\Omega}\tilde{K}_{\Omega 11}\right), \tag{11a}$$

$$\tilde{K}_{\Omega 11} = K^{(0)*}_{-\Omega 11}\left(\tilde{d}_\Omega K_{\Omega 11} + d^*_{-\Omega}\tilde{K}_{\Omega 11}\right), \tag{11b}$$

where $d_\Omega = \kappa^2|\alpha_1|^2 K^{(0)}_{\Omega 22}$ [cf. (A45)] and $\tilde{d}_\Omega = \kappa\alpha_2^*$ [cf. (A43)] are the effective normal and anomalous linear dynamical susceptibilities of the $\chi^{(2)}$ medium near the subharmonic frequency. "Loopless" expressions for the noise sources result in the only nonzero average $\langle \delta\varepsilon'_{\Omega 1}\delta\varepsilon'_{\Omega' 1}\rangle = i\hbar\kappa\alpha_2 \times 2\pi\delta(\Omega+\Omega')$ [cf. (A32) and (A36)] (clearly this violates the classical inequality $\left\langle \left|a\delta\varepsilon'_{\Omega 1} + b\delta\varepsilon'^*_{\Omega' 1}\right|^2\right\rangle \geq 0$). The quantum fluctuations in the subharmonic are thus expressed in terms of the linear response functions [cf. (A40)],

$$G_{\Omega 11} = i\hbar\kappa\alpha_2 K_{\Omega 11}\tilde{K}_{-\Omega 11} + \text{c.c.}, \tag{12a}$$

$$\tilde{G}_{\Omega 11} = i\hbar\kappa\alpha_2 K_{\Omega 11}K_{-\Omega 11} - i\hbar\kappa\alpha_2^*\tilde{K}^*_{\Omega 11}\tilde{K}^*_{-\Omega 11}. \tag{12b}$$

Equations (11) are easily solved:

$$K_{\Omega 11} = \frac{1}{2}\left[L_-(\Omega) + L_+(\Omega)\right], \tag{13a}$$

$$\tilde{K}_{\Omega 11} = \frac{1}{2}\left[L_-(\Omega) - L_+(\Omega)\right]. \tag{13b}$$

Here

$$L_\pm(\Omega) = \left[\Omega + i\gamma_1\left(1 \pm A_2 + i\frac{\gamma_2 A_1^2}{\Omega + i\gamma_2}\right)\right]^{-1} \tag{14}$$

and the dimensionless "dressed" mode amplitudes A_1 and A_2 and field phases are given by the relations

$$\alpha_1 = (\hbar Q)^{\frac{1}{2}} A_1, \quad \alpha_2 = i\,|\alpha_2^c|\,A_2, \tag{15}$$

where

$$|\alpha_2^c| = \frac{\gamma_1}{\kappa}, \quad Q = \frac{\gamma_2}{\gamma_1}N_2^c. \tag{16}$$

The quantities α_2^c and $N_2^c = \hbar^{-1}|\alpha_2^c|^2$ are, respectively, the threshold amplitude and photon number in the fundamental (recall that κ is assumed to be real and positive). The time-normal averages are found to be

$$G_{\Omega 11} = \frac{\hbar}{8\gamma_1}\left[S_-(\Omega) - S_+(\Omega)\right], \tag{17a}$$

$$\tilde{G}_{\Omega 11} = \frac{\hbar}{8\gamma_1}\left[S_-(\Omega) + S_+(\Omega)\right], \tag{17b}$$

where $S_\pm(\Omega) = 4A_2\gamma_1^2|L_\pm(\Omega)|^2$. Note that Planck's constant is present only in the formulas for the time-normal averages. [It is *not* present in the scale factor $(\hbar Q)^{\frac{1}{2}} = \frac{(\gamma_1\gamma_2)^{\frac{1}{2}}}{\kappa}$ for the subharmonic field amplitude and appears in its definition only because we express this factor over the quantum parameter Q.]

The output field statistics for the OPO can be solved by correspondence rules [7,9], noticing that the mode amplitude α_1 is related to the mode energy $\omega_0|\alpha_1|^2$ and thus to the output power $2\gamma_1\omega_0|\alpha_1|^2$. The intraresonator time-normal averages of the subharmonic should therefore be multiplied by $(2\gamma_1\omega_0)^{\frac{1}{2}}$ "per argument" to turn them into the corresponding averages of the emitted light. Adding the strong heterodyne field with phase φ and assuming that the full detection efficiency is unity, the photocurrent spectrum is found to be

$$\frac{\langle|i_\Omega|^2\rangle}{\langle|i_\Omega|^2\rangle_{\text{shot}}} = 1 + S_-(\Omega)\cos^2\varphi - S_+(\Omega)\sin^2\varphi. \tag{18}$$

Clearly all this is in agreement with the results known in the literature [1].

C. "One-loop" approach

When considering corrections to the "linearized" results, we assume that the switching occurs between two possible "above-threshold" steady-state solutions, so that $\alpha_1 = 0$. We shall be looking for the corrections to the below-threshold solution in the linearized approximation. Physically, it implies a gedanken experiment with the OPO starting from zero pumping, the latter being increased to reach the threshold region "from below." The results are then extended up to a point where our approach is no longer valid. Note that initially this gives no idea whether the OPO is considered "below" or "above" the threshold (or even whether these words make sense). Yet we shall see that our investigation is in essence confined to the "below-threshold" OPO.

To simplify the treatment, we compute the diagram loops (cf. the Appendix) with the linear response functions and time-normal averages taken in the linearized approximation. The accuracy of this approach will be discussed below. Under this assumption, the one-loop diagrams are confined to the nonlinear *dynamical* correction to the OPO's properties due to the beating of the probe signal [cf. the definition of the linear response before (7)] with the subharmonic self-radiation. Formally, it means that the quantity d_Ω is modified as [cf. (A42)]

$$d_\Omega = \kappa^2 \int \frac{d\Omega'}{2\pi} G_{\Omega-\Omega' 11} K_{\Omega' 22}, \tag{19}$$

where $K_{\Omega 22}$ is the linear response function on the fundamental. Both $G_{\Omega 11}$ and $K_{\Omega 22}$ here are taken in the linearized approximation. The rest of the above equations, including (12), are not affected. In other words, the self-radiation of the OPO develops exactly as does the external signal: the fact that it interacts with itself has no effect on the result. This means that we have only taken into account the first nonvanishing correction in the intensity of the system's self-radiation.

First, if $\alpha_1 = 0$, the linearized theory yields $K_{\Omega 22} = K^{(0)}_{\Omega 22}$. Second, if the medium's nonlinearity is not too high, $Q \gg 1$, the corrections sought are essential only in the near-threshold region. Assuming that $|1 - A_2| \ll \min(1, \frac{\gamma_2}{\gamma_1})$ and $A_1^2 \ll \min(1, \frac{\gamma_2}{\gamma_1})$, the behavior of the system is dominated by the only pole of the response function at $\Omega = -i\Gamma \approx -i\gamma_1(1 - A_2 + A_1^2)$, $\Gamma \ll \gamma_1, \gamma_2$ (the reason why this expression is formally written for $\alpha_1 \neq 0$ becomes clear below). By retaining only this dominating pole term, one finds in the threshold region,

$$G_{\Omega 11} \approx \tilde{G}_{\Omega 11} \approx \hbar Q q \frac{2\Gamma}{\Omega^2 + \Gamma^2}, \tag{20}$$

where $q = \frac{A_2\gamma_1}{4Q\Gamma}$. Since $\Gamma \ll \gamma_2$, we find that $d_\Omega \approx \kappa^2 \hbar Q q K^{(0)}_{\Omega 22}$, which clearly coincides with the "above-threshold" expression for this quantity in the linearized approximation with $\alpha^2_{1\text{eff}} = \hbar Q q$.

Thus, in our approximations the equations for the linear response functions of the subharmonic coincide with those in the linearized approximation within the formal replacement $A_1^2 \leftrightarrow A^2_{1\text{eff}} = q$, while the relations expressing the time-normal averages remain unaffected. Then, we can simply take the "linearized" expressions for these quantities written above (for $\alpha_1 \neq 0$) and replace in them A_1^2 by q. In turn, this allows Γ and q to be defined self-consistently as $\Gamma = \gamma_1(1 - A_2 + q)$ and $q = \dfrac{A_2}{4Q(1 - A_2 + q)}$.

The equations for the response functions and time-normal averages contain the pump only through "dressed" field amplitudes α_1 and α_2 (this allowed them to be viewed as independent). Consider now the equation for the steady-state field amplitude on the fundamental. In the linearized approximation, it is $A_2 = A_2^{(0)} - \frac{A_1^2}{2}$ [cf. (A46) and (A47)], where the dimensionless "bare" field amplitude $A_2^{(0)}$ is defined as the value of A_2 at $\kappa = 0$, i.e., in the empty resonator under the same pumping conditions. The phases of the bare and dressed fields coincide. In the one-loop approximation, the difference between A_2 and $A_2^{(0)}$ is due to the integral amplitude of the anomalous correlations in the subharmonic, which are "processed" into the coherent signal in the fundamental by the OPO's nonlinearity [cf. (A48)]. Since $\int \frac{d\Omega}{2\pi} \tilde{G}_{\Omega 11} = \hbar Q q$, again this results in the replacement $A_1^2 \to q$, and the equation for the average amplitude on the fundamental is found to be $A_2 = A_2^{(0)} - \frac{q}{2}$. The phase conditions remain unaffected. This completes the set of nonlinear equations expressing A_2 and q by $A_2^{(0)}$. However, for practical purposes it is convenient to consider $A_2^{(0)}$ and A_2 as functions of the quantum "noise" parameter q, which leads to rational relations: $A_2 = \dfrac{4Qq(1+q)}{1+4Qq}$ and $A_2^{(0)} = A_2 + \frac{q}{2}$. Both these are monotone functions of q.

III. RESULTS AND DISCUSSION

Let us first discuss the accuracy of our results. The approximations used contain three successive steps: (i) the one-loop approach, (ii) the assumption that the loops may be computed with the "lines" taken in the linearized approximation, and (iii) the condition

$$\Gamma \ll \gamma_2, \tag{21}$$

allowing for the "one-pole" self-consistent computational scheme. It is easy to see that our approach as a whole is consistent if $1 - A_2 \gg q$ or, equivalently,

$$1 - A_2^{(0)}, 1 - A_2 \gg \frac{1}{2Q^{\frac{1}{2}}} \gg q. \tag{22}$$

The important question is whether our approach implies any loss in accuracy compared with that of the "one-loop" Dyson equations themselves. Simple qualitative considerations show that this is not the case. It is obvious that the expression for the leading pole of the linear response functions, $\Gamma \approx \gamma_1(1 - A_2 + q)$, is the truncated expansion of this quantity over the powers of the critical-noise parameter q, $\Gamma = \gamma_1(1 - A_2 + \sum_{k=1}^{\infty} c_k q^k)$. To produce c_k, the succeptibilities and noise sources in

the Dyson equations should include all essential n-loop diagrams for $n \leq k$ (assuming that the diagrams are expressed over the "dressed" lines and "bare" vertices; cf. [10]). As is shown in the Appendix, the one-loop Dyson equations miss already some essential two-loop diagrams, i.e., these equations cannot produce c_k for $k > 1$. It means that our approximation exhausts their accuracy. Direct evaluation of the "missed" diagrams presented in the Appendix leads to the same conclusion.

Note, however, that all these considerations imply condition (21). If this condition does not hold, the "one-pole" approach breaks down, but the one-loop Dyson equations themselves may remain valid.

We see that the "number-of-loops" expansion is not the system-size expansion. In the threshold region, the true large parameter of the problem is

$$P = (1 - A_2)^2 \frac{\gamma_2}{\gamma_1} N_2^c \tag{23}$$

(this parameter emerges also in the estimates of the "missed" diagrams, cf. the Appendix). This is substantially different from the system-size parameter $N_2^c = \hbar^{-1} |\alpha_2^c|^2 = \frac{\gamma_1^2}{\hbar \kappa^2}$: the condition $N_2^c \gg 1$ is necessary but not sufficient.

It may be expected that the results are still qualitatively correct up to the point where

$$1 - A_2 = q. \tag{24}$$

For $Q \gg 1$, this corresponds to $1 - A_2 = q \approx \frac{1}{2(2Q)^{\frac{1}{2}}}$ and $1 - A_2^{(0)} \approx \frac{1}{4(2Q)^{\frac{1}{2}}}$. This turns out to be consistent with [11], where the precise solution for the quantum state of the subharmonic was obtained in the adiabatic limit $\gamma_2 \gg \gamma_1$. Following [11], the threshold region for the OPO (characterized by the growth of the subharmonic fluctuations) can be estimated to be at $1 - A_2^{(0)} \sim \frac{1}{Q^{\frac{1}{2}}}$, this being in agreement with our results.

Note that in the antiadiabatic case, i.e., if $\frac{\gamma_2}{\gamma_1} \ll 1$, we must also assume that $\frac{\gamma_2}{\gamma_1} \gg \frac{1}{2(2Q)^{\frac{1}{2}}}$, so as to preserve the condition $\Gamma \ll \gamma_2$.

The fact that the "one-loop" relations are formally found by substituting q for A_1^2 in the "linearized" relations has a transparent physical interpretation. The approximate values (20) of the time-normal averages describe a field in a classical state with well-defined *square* of the amplitude, $\alpha_{1\text{eff}}^2 = \hbar Q A_{1\text{eff}}^2 = \hbar Q q$. The sign of the amplitude is uncertain, and changes randomly with the characteristic time Γ^{-1}. This noise is nothing but the fluctuations in the subharmonic radiation's antisqueezed quadrature. On the time scales $\tau \ll \Gamma^{-1}$ it is indistinguishable from the coherent subharmonic field with $\alpha_1 = \alpha_{1\text{eff}} = \pm (\hbar Q q)^{\frac{1}{2}}$, this being exactly the result found above (recall that $\gamma_2 \gg \Gamma$ was assumed). This interpretation agrees also with the structure of the diagrams [cf. (A49)].

On the one hand, $\alpha_1 = 0$, which is characteristic of the below-threshold solution in the linearized approximation. On the other hand, $\alpha_{1\text{eff}}^2 \neq 0$, which is characteristic of the above-threshold one. So, while remaining below threshold [cf. (22)], we nevertheless see the seed of the above-threshold solution—provided the subharmonic fluctuations are essential in the OPO's dynamics, it is uncertain whether the OPO is "below" or "above" threshold.

This emphasizes that for the OPO the very concept of threshold is qualitative rather than quantitative. In the present solution "from below," the threshold region is defined by the growth of the subharmonic fluctuations. At the same time, this solution casts into doubt the very possibility of a definition "from above." On the one hand, the threshold region is naturally defined as a region where critical fluctuations in the OPO are essential. On the other hand, we found that the coherent subharmonic steady-state amplitude is exactly the critical subharmonic noise. It must be the case in the "above-threshold" region as well, so that this region is characterized by further growth of critical fluctuations in the OPO rather than by their decrease. From this perspective, if the OPO is not "below" the threshold, i.e., if the critical fluctuations cannot be regarded as being negligible, it is *ipso facto* "above" the threshold.

As far as the OPO's dynamics is concerned, the OPO's self-radiation acts as a strong classical noise. Not surprisingly, its presence degrades the quantum properties of the OPO. For example, the subharmonic is no longer in a minimum uncertainty state, for, whereas $U(\Omega) = [1 - S_+(\Omega)][1 + S_-(\Omega)] = 1$, it is easy to see that

$$U(0) = \left[1 - \frac{4A_2 q}{(1 + A_2 + q)^2}\right]\left[1 + \frac{4A_2 q}{(1 - A_2 + q)^2}\right] > 1.$$

The noise of the OPO affects substantially the uncertainty of the state of the subharmonic if $1 - A_2^{(0)} \gg \frac{1}{(4Q)^{\frac{1}{3}}}$. This does not contradict condition (22), i.e., the subharmonic already ceases to be in a minimum-uncertainty squeezed state in the domain of quantitative validity of the results. For the "edge of applicability" condition (24), $U(0) \approx 2(2Q)^{\frac{1}{2}} \gg 1$.

The squeezing spectrum in the output signal is given by

$$S_+(\Omega) = 4A_2\gamma_1^2 \left|\Omega + i\gamma_1 \left(1 + A_2 + \frac{iq\gamma_2}{\Omega + i\gamma_2}\right)\right|^{-2}. \tag{25}$$

Depending on the values of the parameters, the dynamical corrections can either "flatten the bottom" of the squeezing spectrum [Fig. 1(a)] or even give it the two-minima shape characteristic of the "above-threshold" OPO [Fig. 1(b)]. One can check that if $\frac{\gamma_2}{\gamma_1} \geq \left(\frac{2}{Q}\right)^{\frac{1}{4}}$, the two-minima shape is not achieved within the domain of applicability of the results. The maximum squeezing is observed then at $\Omega = 0$ and is independent of the ratio $\frac{\gamma_2}{\gamma_1}$. It is shown in Fig. 2 as a function of the pumping for different values of Q. The span of the curves is from the zero pumping to that corresponding to condition (24). Figure 2 clearly indicates the existence of

an optimal pumping allowing for a maximum squeezing within the domain of the applicability of the results. It is easy to find that this is achieved at the following values of the parameters:

$$q_{\text{opt}} = \frac{1}{2(2Q)^{\frac{2}{3}}} + O\left(\frac{1}{Q^{\frac{4}{3}}}\right), \tag{26a}$$

$$A_{2\text{opt}} = 1 - \frac{1}{(2Q)^{\frac{1}{3}}} + \frac{3}{2(2Q)^{\frac{2}{3}}} + O\left(\frac{1}{Q}\right), \tag{26b}$$

$$A^{(0)}_{2\text{opt}} = 1 - \frac{1}{(2Q)^{\frac{1}{3}}} + \frac{7}{4(2Q)^{\frac{2}{3}}} + O\left(\frac{1}{Q}\right), \tag{26c}$$

$$S_+(0)_{\text{opt}} = 1 - \frac{3}{4(2Q)^{\frac{2}{3}}} + \frac{1}{8Q} + O\left(\frac{1}{Q^{\frac{4}{3}}}\right). \tag{26d}$$

These results are valid if $2(2Q)^{\frac{1}{3}} \gg 1$, the condition being well satisfied in practice.

Note that the optimal squeezing is located exactly where the noise of the OPO starts to affect the quantum uncertainty of the state of the subharmonic. Undoubtedly this is not just a coincidence. Both effects have the same physical origin, namely, the dynamical effect of the critical fluctuations in the OPO in the near-threshold region.

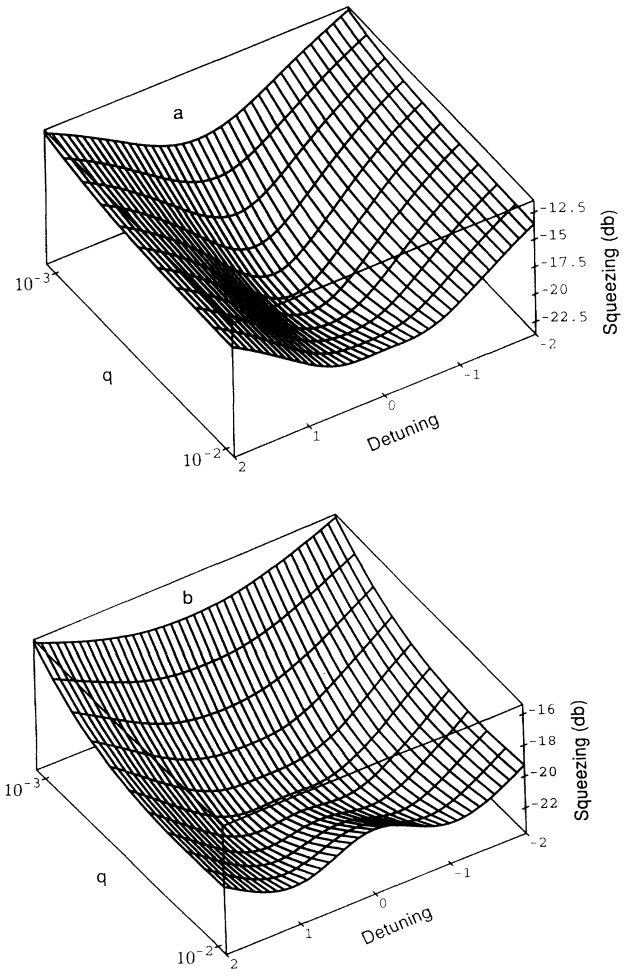

FIG. 1. Dependence of the shape of squeezing spectrum on the pumping. $Q = 10^3$, $\gamma_1 = 1$. (a) $\gamma_2 = 0.21$; (b) $\gamma_2 = 0.11$.

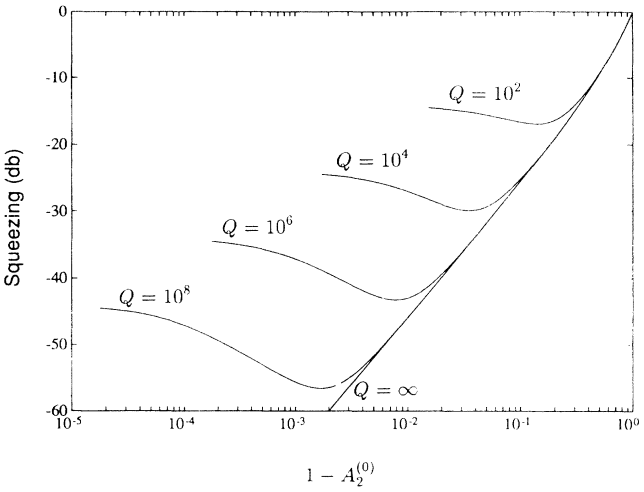

FIG. 2. Dependence of the maximum squeezing on the pumping conditions.

If $\frac{\gamma_2}{\gamma_1} < \left(\frac{2}{Q}\right)^{\frac{1}{4}}$, the dynamical corrections can give the squeezing spectrum the two-minima shape [Fig. 1(b)]; cf. [3]. This happens if the parameters obey the condition $\frac{\gamma_2}{\gamma_1} < [2(1 + A_2)q]^{\frac{1}{2}}$. Recall that we are not allowed to make $\frac{\gamma_2}{\gamma_1}$ arbitrarily small, because the condition $\gamma_2 \gg \Gamma = \gamma_1(1 - A_2 + q)$ must hold for our results to be consistent. Thus the predictions about the shape of the squeezing spectrum are reliable in the band of pumpings, $\frac{\gamma_2}{\gamma_1} \gg 1 - A_2^{(0)} \gg \frac{1}{2(2Q)^{\frac{1}{2}}}$. This contains also the above-mentioned condition, $\frac{\gamma_2}{\gamma_1} \gg \frac{1}{2(2Q)^{\frac{1}{2}}}$, which makes the results applicable. Assuming a slightly stronger condition, $\frac{\gamma_2}{\gamma_1} \gg \frac{1}{2(2Q)^{\frac{1}{3}}}$, the "band of consistency" covers the optimal-squeezing region as well. It is then easy to see that the squeezing spectrum takes on the two-minima shape only for pumpings greater than optimal [cf. Fig. 1(b)]. Indeed, the converse would require $\frac{\gamma_2}{\gamma_1} < [2(1 + A_{2\text{opt}})q_{\text{opt}}]^{\frac{1}{2}}$, the condition contradicted by the assumed one. As such, the two-minima shape of the spectrum appears only when the squeezing has already been degraded by the critical fluctuations in the OPO and does not affect the estimate of the optimal squeezing.

Our results reveal that some of the conclusions made in [12] do not apply to the spectral properties of squeezing. In that paper, general limitations to the squeezing achievable by means of an optical parametric amplifier were considered. It was shown that there exists a general limit to the total squeezing which scales as $N_2^{-\frac{1}{2}}$ with the number of photons in the pump mode N_2. Assuming that $\gamma_1 = \gamma_2$ and $A_{2\text{opt}} \approx A^{(0)}_{2\text{opt}} \approx 1$ the maximum squeezing

given by (26d) scales with N_2 as $1-S_+(0)_{\rm opt} \sim N_2^{-\frac{2}{3}}$. So the limit $N_2^{-\frac{1}{2}}$ is not applicable to the maximal *spectral* squeezing.

Let us now compare our results with Ref. [3] where the squeezing spectra were obtained by means of numerical solution of the one-loop Dyson equations. The equations used in [3] are formally equivalent to those on which our approach is based, so that comparing our results with [3] provides us with a direct check of our approximations. In Fig. 3 we present the squeezing spectra as given by relation (25). The values of the parameters are chosen so as to match exactly the corresponding Fig. 11(a) in [3], namely, $\gamma_2 = 0.1\gamma_1$ and $A_2 = 0.95$. [There is some confusion in [3] concerning the threshold parameter defined as $p = \frac{\kappa\varepsilon_2}{\gamma_1\gamma_2}$. Since $\frac{\varepsilon_2}{\gamma_2}$ is the bare amplitude of the fundamental, $\left|\alpha_2^{(0)}\right|$, and $\frac{\gamma_1}{\kappa} = \alpha_2^c$, in our terms $p = \left|\frac{\alpha_2^{(0)}}{\alpha_2^c}\right| = A_2^{(0)}$. However, its place in the Dyson equations in [3] is consistent only with $p = A_2$. We assume $p = A_2$.] The results of [3] are also replotted in Fig. 3. Curve c ($Q = 1000, q = 0.003$) exhibits obvious quantitative agreement with the corresponding curve in [3] even though the condition $\gamma_2 \gg \Gamma$ is not very well satisfied ($\gamma_2 = 0.1\gamma_1$ and $\Gamma = 0.05\gamma_1$). This shows that condition (21) is not critical. Another two curves in Fig. 3, corresponding to $Q = 100$ ($q = 0.011$) and $Q = 60$ ($q = 0.016$), respectively, exhibit only qualitative agreement with [3]. However, for these parameters condition (22) does not strictly hold, and we are outside the validity of our approach.

Obvious disagreement of our results with that found by Zaidi [2] is probably due to the fact that instead of the actual Dyson equation Zaidi used graphical relations of unclear origin. Apparently, these are invalid because of the overlapping of diagrams. In any case, the consistency of the quantum-field-theoretical results presented in [3] and in this paper with those found by a completely different method in [11] leaves little doubt that the results of Zaidi are erroneous.

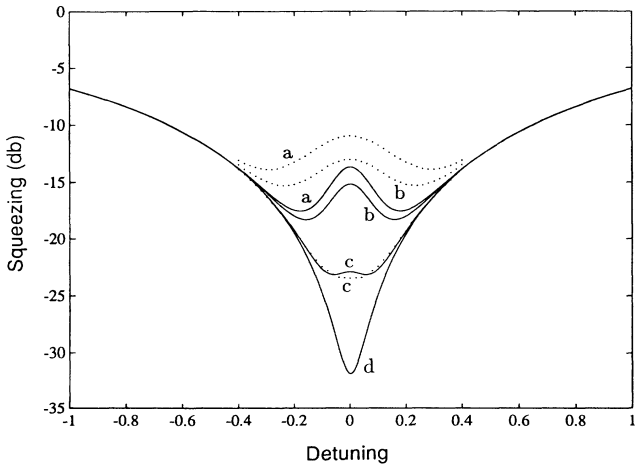

FIG. 3. Squeezing spectra for $A_2 = 0.95$, $\gamma_1 = 1$, and $\gamma_2 = 0.1$. (a) $Q = 60$; (b) $Q = 100$; (c) $Q = 1000$; (d) linearized theory. The solid lines represent our results and the dotted lines represent the results of [3].

In conclusion, it has been shown that close to the threshold quantum properties of the degenerate OPO are degraded by the fluctuations in the antisqueezed quadrature of the subharmonic noise, the effect which is in essence classical. In particular, this results in the existence of the optimal pumping conditions providing for the maximum squeezing.

ACKNOWLEDGMENTS

We are grateful to Dr. B. Kennedy for providing us with prepublication information for Ref. [3] and to Professor G. Stedman for comments on the manuscript. One of us (L.P.) is grateful to Professor R. Keam for discussions on the formal approach. This research was supported by the New Zealand Foundation for Research, Science and Technology, the University of Auckland Research Committee, and the New Zealand Lottery Grants Board.

APPENDIX: CAUSAL DIAGRAM TECHNIQUES FOR NONLINEAR OPTICAL SYSTEMS

1. Quantum input-output approach

Let the time-normal ordering be defined for an arbitrary time-dependent operator $\boldsymbol{O}(x,t)$ as

$$\langle T_N F(\boldsymbol{O})\rangle = F(i\frac{\delta}{\delta\zeta})\left\langle T_- \exp\left[-i\zeta^{(+)}\boldsymbol{O}\right] \times T_+ \exp\left[-i\zeta^{(-)}\boldsymbol{O}\right]\right\rangle\Big|_{\zeta=0}, \qquad \text{(A1)}$$

where T_+ is the Dyson time ordering, T_- is the reverse ordering, $T_-(\cdots) = \{T_+[(\cdots)^\dagger]\}^\dagger$, the "products" are "scalar" ones,

$$\zeta^{(\pm)}\boldsymbol{O} = \int dx\, dt \zeta^{(\pm)}(x,t)\boldsymbol{O}(x,t), \qquad \text{(A2)}$$

and $(\cdots)^{(\pm)}$ means taking the frequency-positive and negative parts [Fourier transforms are $f_\omega = \int dt f(t)\exp i\omega t$ and $f(t) = (2\pi)^{-1}\int d\omega f_\omega \exp(-i\omega t)$]. (A1) is equivalent to the conventional definition [5] within the approximation of slowly varying amplitudes. Its refinement beyond this approximation is justified by the results below.

Let now $\tilde{\boldsymbol{A}}(x,t)$ be the Heisenberg field operator defined in the presence of an external current $j_{\rm ext}(x,t)$, i.e., where the interaction Hamiltonian is of the form

$$H_{\rm int}(t) = \int dx \tilde{\boldsymbol{A}}(x,t)\left[\tilde{\boldsymbol{J}}(x,t) + j_{\rm ext}(x,t)\right], \qquad \text{(A3)}$$

and where $\tilde{\boldsymbol{J}}(x,t)$ is the Heisenberg current operator and x includes all field degrees of freedom. In the notation used in [7], $\tilde{\boldsymbol{A}} = \boldsymbol{A}^{(\mathrm{ext})}\big|_{a_{\mathrm{ext}}=0}$ and $\tilde{\boldsymbol{J}} = \boldsymbol{J}^{(\mathrm{ext})}\big|_{a_{\mathrm{ext}}=0}$. Operators defined in the absence of the source bear no tilde, $\boldsymbol{A}(x,t) = \tilde{\boldsymbol{A}}(x,t)|_{j_{\mathrm{ext}}=0}$ and $\boldsymbol{J}(x,t) = \tilde{\boldsymbol{J}}(x,t)|_{j_{\mathrm{ext}}=0}$. The following precise relation holds with arbitrary c-number function $\zeta(x,t)$ [7],

$$\left\langle T_N \exp\left(-i\zeta\tilde{\boldsymbol{A}}\right)\right\rangle = \langle T_- \exp(i\eta_-\boldsymbol{A}) \times T_+ \exp(-i\eta_+\boldsymbol{A})\rangle \tag{A4}$$

where

$$\eta_\pm(x,t) = \hbar^{-1} j_{\mathrm{ext}}(x,t) \pm \zeta^{(\mp)}(x,t). \tag{A5}$$

Thus the knowledge of the time-normal averages of the field operator in the presence of an arbitrary external source is equivalent to the conventional quantum description of a quantum electromagnetic system (see [7] for the relations accounting for the currents). Under macroscopic conditions, this kind of description corresponds to the input-output description of real devices [7], i.e., (A4) provides the rigorous solution of the quantum input-output problem [8,9,13]. Among the relations following from (A4) one finds, e.g., Kubo's fluctuation-dissipation theorem for an electromagnetic system [4],

$$\left.\frac{\delta\left\langle\tilde{\boldsymbol{A}}(x,t)\right\rangle}{\delta j_{\mathrm{ext}}(x',t')}\right|_{j_{\mathrm{ext}}=0} = -i\hbar^{-1}\theta(t-t')\left\langle[\boldsymbol{A}(x,t),\boldsymbol{A}(x',t')]\right\rangle. \tag{A6}$$

2. Causal diagram techniques

Viewed as a functional over the c-number functions $\eta_+(x,t)$ and $\eta_-(x,t)$, the quantum average on the right of (A4) is exactly the characteristic functional of the Perel-Keldish-type [6] quantum field averages:

$$\langle T_- \boldsymbol{A}(x_1,t_1)\cdots\boldsymbol{A}(x_m,t_m) \times T_+ \boldsymbol{A}(x'_1,t'_1)\cdots\boldsymbol{A}(x'_n,t'_n)\rangle$$

$$= i^{n-m}\left.\frac{\delta^{m+n}\langle T_- \exp(i\eta_-\boldsymbol{A}) \times T_+ \exp(-i\eta_+\boldsymbol{A})\rangle}{\delta\eta_-(x_1,t_1)\cdots\delta\eta_-(x_m,t_m)\,\delta\eta_+(x'_1,t'_1)\cdots\delta\eta_+(x'_m,t'_m)}\right|_{\eta_+=\eta_-=0}. \tag{A7}$$

Relation (A4) then rearranges Perel-Keldish's diagram series [6] so as to produce the quantum statistical "macroscopic-response" functions,

$$K^{(m,n)}(x_1,t_1,\cdots,x_m,t_m;x'_1,t'_1,\cdots,x'_n,t'_n) = \left.\frac{\delta^n\left\langle T_N\tilde{\boldsymbol{A}}(x_1,t_1)\cdots\tilde{\boldsymbol{A}}(x_m,t_m)\right\rangle}{\delta j_{\mathrm{ext}}(x'_1,t'_1)\ldots\delta j_{\mathrm{ext}}(x'_n,t'_n)}\right|_{j_{\mathrm{ext}}=0}. \tag{A8}$$

These functions obey natural causality conditions ($n \neq 0$) [7]:

$$K^{(m,n)}(x_1,t_1,\ldots,x_m,t_m;x'_1,t'_1,\ldots,x'_n,t'_n) = 0 \text{ if } t_r < t'_s \text{ for all } r,s. \tag{A9}$$

Consider first the propagator in this new diagram technique. Applied to a linear passive (i.e., nonradiating) system, relation (A4) yields

$$D_F(x,x',\tau) = D^{(+)}_{\mathrm{ret}}(x,x',\tau) + D^{(+)}_{\mathrm{ret}}(x',x,-\tau), \tag{A10a}$$

$$D(x,x',\tau) = D^{(+)}_{\mathrm{ret}}(x,x',\tau) - D^{(+)*}_{\mathrm{ret}}(x',x,-\tau), \tag{A10b}$$

where with $A(x,t)$ being the free-field operator and $|0\rangle$ being the free-field vacuum

$$D_F(x,x',t-t') = -i\hbar^{-1}\langle 0|T_+A(x,t)A(x',t')|0\rangle, \tag{A11a}$$

$$D(x,x',t-t') = -i\hbar^{-1}\langle 0|A(x,t)A(x',t')|0\rangle \tag{A11b}$$

are the constituents of the matrix propagator in Perel-Keldish's techniques, and

$$D_{\mathrm{ret}}(x,x',t-t') = -i\hbar^{-1}\theta(t-t')[A(x,t),A(x',t')] \tag{A12}$$

is the linear response function of the linear system [cf. (A6)]. As was shown in [7], D_{ret} is nothing but the retarded Green's function of the classical (c-number) inhomogeneous wave equation in the linear medium. So propagator (A12) in this new diagram technique is a fully classical quantity with natural causal properties. The whole system's quantum properties are thus due exclusively to its nonlinearity—by themselves, the free-field's quantum properties are unobservable.

Instead of actually rearranging the Perel-Keldish's series, it is much easier to derive directly the techniques

sought following the general relation existing between the closed perturbation formulas and graphical approaches [10]. Such a formula corresponding to Perel-Keldish's series was derived in [7]. After the transformation induced by (A4), and being confined to the field averages, it takes the form

$$\left\langle T_N \exp\left(-i\zeta\tilde{\boldsymbol{A}}\right)\right\rangle = \exp(\Delta)\, G(\chi,a)|_{\chi=a=0}\,, \tag{A13}$$

where

$$\Delta = \int dx\, dx'\, dt\, dt' \left[\frac{\delta}{\delta a(x,t)} - i\zeta(x,t)\right] D_{\rm ret}(x,x',t-t') \left[i\frac{\delta}{\delta\chi(x',t')} + j_{\rm ext}(x',t')\right], \tag{A14}$$

$$G(\chi,a_e) = \left\langle T_- \exp i\left(-\chi^{(+)} + \hbar^{-1}a\right) J \times T_+ \exp i\left(-\chi^{(-)} - \hbar^{-1}a\right) J\right\rangle \tag{A15}$$

and $J(x,t)$ is the current operator in the interaction picture.

Relation (A13) generates the diagram techniques sought with the propagator $D_{\rm ret}$ and the "bare" vertices

$$V^{(m,n)}(x_1,t_1,\ldots,x_m,t_m;x_1',t_1',\ldots,x_n',t_n') = i^m \frac{\delta^{m+n}\ln G(\chi,a)}{\delta\chi(x_1,t_1)\cdots\delta\chi(x_m,t_m)\delta a(x_1',t_1')\cdots\delta a(x_n',t_n')}\bigg|_{\chi=a=0}. \tag{A16}$$

The overall factor for a diagram is real and confined to the standard symmetry coefficient [10]; no complex factors characteristic of conventional quantum approaches occur. Vertices (A16) obey the causality condition (A9), cf. Ref. [7], appendix B. The structure of the diagrams is also governed by causality: the "earlier" and "later" ends of the propagator are always connected to the "outputs" and "inputs" of the vertices, respectively. Since the diagram lines correspond to causal propagating waves (this replacing a rather murky concept of virtual photon), the causality condition (A9) holds for individual diagrams, a result which provides new insight into the quantum properties of nonlinear electromagnetic systems. In particular, all diagrams containing a subdiagram with the structure $K^{(0,n)}$ are precisely equal to zero (cf. Perel's cancellation rule [6]).

To illustrate the way in which the diagrams will be drawn, consider, for example, the first nonvanishing approximation to the response function $K^{(2,1)}$,

$K^{(2,1)} =$ 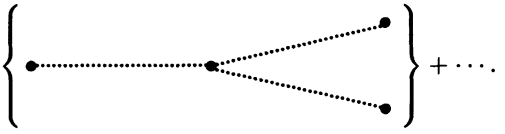 $+\cdots.$

(A17)

Here, the dotted lines and the point in which they are connected denote the propagator $D_{\rm ret}$ and the vertex $V^{(2,1)}$, respectively. To make our graphical notation unambiguous, we assume that the "inputs" of any graphical object point to the left and the "outputs" point to the right (note that this is opposite to the direction of the "time flow" in analytical expressions, $a = D_{\rm ret}j$, say). When a diagram in the frequency domain is considered, this convention applies to its structure before taking the Fourier transform. The symmetry coefficients for the diagram will be shown explicitly [in (A17) it is equal to one]. The curly brackets are intended to improve the readibility of the formulas containing graphical objects (they can also be considered as mapping of the diagram on the corresponding expression).

When the system's nonlinearity is described phenomenologically by the effective "interaction" Hamiltonian $H_{\rm int}(t)$, the above results apply with

$$\ln G(\chi,a) = i\hbar^{-1}\int dt\Big\{\mathcal{H}_{\rm int}\left[-\hbar\chi^{(+)}(x,t) + a(x,t)\right] - \mathcal{H}_{\rm int}\left[\hbar\chi^{(-)}(x,t) + a(x,t)\right]\Big\}, \tag{A18}$$

where $\mathcal{H}_{\rm int}$ is the symmetric representation of $H_{\rm int}(t)$,

$$H_{\rm int}(t) = {\rm sym}\left\{\mathcal{H}_{\rm int}\left[\boldsymbol{A}(x,t)\right]\right\}. \tag{A19}$$

Relation (A18) might also be helpful when deriving an effective field self-action from a microscopic atomic model.

Relation (A13) with $\ln G(\chi,a)$ given by (A18) may produce the diagrams where some of the lines start and finish on the same vertex. In general, these diagrams are characteristic of non-Markovian systems. Since the field self-action described by an effective Hamiltonian is Markovian, these diagrams should be ignored in the quasiresonance approximation. Indeed, on the one hand, the system's properties cannot depend on the small delay introduced into $D_{\rm ret}$; on the other hand, this delay makes the diagrams with "short-circuited" lines equal to zero. Beyond the quasiresonant approximation, this problem is outside the scope of this paper.

3. Classical interpretation of the diagram series

The perturbation relation (A13) lacks Planck's constant and therefore must have a classical analog [7]. As a result, the fundamental property of the diagram series obtained is that they are representations of nonlinear statistical c-number electrodynamics. Consider a classi-

cal system consisting of the set of linear and nonlinear devices. Let the linear devices be characterized by the retarded Green's function $D_{\rm ret}$ and the nonlinear ones described in terms of the random current $j'(x,t)$ (currents in linear devices are not observed directly). Microscopically, the nonlinear statistical properties of this system may be determined by the nonlinear statistical susceptibilities $V^{(m,n)}$:

$$\langle\langle j'(x_1,t_1)\cdots j'(x_m,t_m)\rangle\rangle = \sum_{n=0}^{\infty}\frac{1}{n!}\int dx_1'dt_1'\cdots dx_n'dt_n'V^{(m,n)}(x_1,t_1,\ldots,x_m,t_m;x_1',t_1',\ldots,x_n',t_n') \times\langle\langle a(x_1',t_1')\cdots a(x_n',t_n')\rangle\rangle, \tag{A20}$$

where $a(x,t)$ is the full random microscopic field and double angle brackets denote classical statistical averaging. Macroscopically, these properties may be described in terms of the statistical response functions $K^{(m,n)}$ relating the statistical properties of the full field to the influence of an external current $j_{\rm ext}$, so that

$$a(x,t) = \int dx'dt'D_{\rm ret}(x,x',t-t')\,[j'(x',t') + j_{\rm ext}(x',t')] \tag{A21}$$

and

$$\langle\langle a(x_1,t_1)\cdots a(x_m,t_m)\rangle\rangle = \sum_{n=0}^{\infty}\frac{1}{n!}\int dx_1'dt_1'\cdots dx_n'dt_n'K^{(m,n)}(x_1,t_1,\ldots,x_m,t_m;x_1',t_1',\ldots,x_n',t_n') \times j_{\rm ext}(x_1',t_1')\cdots j_{\rm ext}(x_n',t_n'). \tag{A22}$$

The connection between the microscopic susceptibilities and the macroscopic statistical response functions is the classical self-action problem. Following the analysis of the quantum-classical correspondences presented in [7], it can be checked that if the classical susceptibilities (A20) were substituted for vertices (A16) in the causal diagram series, these would produce precisely the classical macroscopic response functions (A22).

For example, from the classical point of view, diagram (A17) describes a noise radiation excited by a coherent field initially emitted by an external source. The external field propagates in the medium (the leftmost line) and creates a polarization of a noise nature (the vertex). In turn, the noise field emitted by the noise polarization propagates in the medium (the two rightmost lines).

Importantly, if vertices (A16) may be interpreted as susceptibilities (A20), the quantum system becomes both formally and physically indistinguishable from the respective classical system. The "quantum difference" therefore resides only in the impossibility to interpret some of the quantum "susceptibilities" (A16) in classical statistical terms. This is always connected with the nonclassical nature of the system's noise properties—the *dynamics* of the macroscopic quantum optical systems is fully classical. In particular, the linear field damping can always be considered in classical terms. Indeed, it is connected with vertex $V^{(1,1)}$, the classical interpretation of which is valid unconditionally. Note also that vertex $V^{(2,0)}$ fully accounts for the self-radiation of a linear heat bath ("hot" or "squeezed" reservoirs).

4. Dyson equations for the one- and two-point quantum statistical averages

Since the established diagram series themselves consist of the standard Feynman-type graphs, the whole of the usual approaches to graphical techniques is applicable [10]. In particular, the following graphical (Dyson) equations hold:

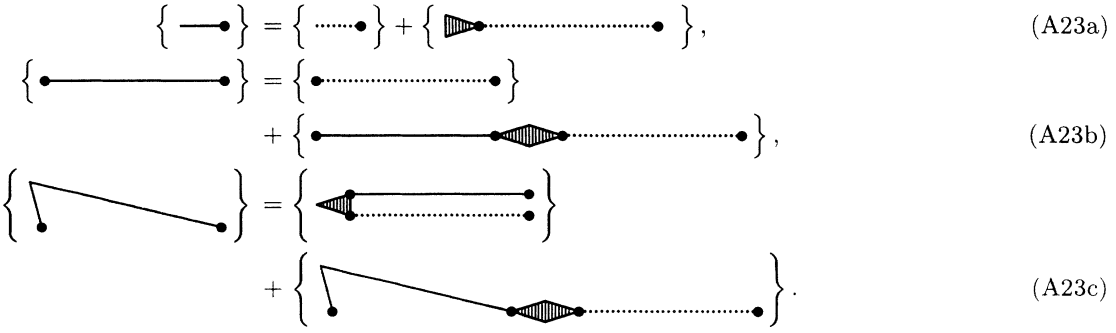

(A23a)

(A23b)

(A23c)

Here,

$$\left\{ \quad \right\} = K^{(1,0)}(x,t) = \langle \boldsymbol{A}(x,t) \rangle \tag{A24}$$

is the average ("dressed") field,

$$\left\{ \quad \right\} = K^{(1,1)}(x,t;x',t') \tag{A25}$$

is the linear response function (A6),

$$\begin{aligned} \left\{ \quad \right\} &= K^{(2,0)}(x,t,x',t') - K^{(1,0)}(x,t)K^{(1,0)}(x',t') \\ &= \langle T_N \boldsymbol{A}(x,t)\boldsymbol{A}(x',t') \rangle - \langle \boldsymbol{A}(x,t) \rangle \langle \boldsymbol{A}(x',t') \rangle \end{aligned} \tag{A26}$$

is the connected (incoherent) part of the two-point time-normal average. The dotted line denotes the causal propagator D_{ret} and $\left\{ \quad \right\}$ is the "bare" field, i.e., the average field in the empty resonator for the same pumping conditions. Importantly, the only informative detail as to how the "dressed" graphical objects are drawn is whether their ends point to the right or to the left. All other details of their shape, including bends, must be ignored.

It is easy to check that Eq. (A23c) is satisfied by

$$\left\{ \quad \right\} = \left\{ \quad \right\}. \tag{A27}$$

This is exactly relations (8) which thus are very general.

Relations (A23) are nothing but the inhomogeneous wave equations with the average polarization $\left\{ \quad \right\}$, linear susceptibility $\left\{ \quad \right\}$ and noise-polarization source $\left\{ \quad \right\}$. Thin lines denote their arguments. These are *macroscopically observable* quantities unlike the "bare" vertices $V^{(1,0)}$, $V^{(1,1)}$, and $V^{(2,0)}$. Provided that the average polarization and susceptibility are viewed as given quantities, Eqs. (A23a) and (A23b) are fully classical. This is not the case for relation (A23c) [or (A27)] where the interpretation of the "noise source" in classical statistical terms may be impossible (yet these relations may always be regarded as being structurally classical).

The quantum "sources" may be expressed as diagram series in terms of the quantities (A24), (A25), and (A26),

$$\left\{ \quad \right\} = \tfrac{1}{2} \left\{ \quad \right\} + \tfrac{1}{2} \left\{ \quad \right\} + \cdots, \tag{A28a}$$

$$\left\{ \quad \right\} = \left\{ \quad \right\} + \tfrac{1}{2} \left\{ \quad \right\} + \left\{ \quad \right\} + \cdots, \tag{A28b}$$

$$\left\{ \quad \right\} = \left\{ \quad \right\} + \tfrac{1}{2} \left\{ \quad \right\} + \left\{ \quad \right\} + \left\{ \quad \right\} + \cdots. \tag{A28c}$$

The diagrams shown explicitly correspond to the one-loop approximation to the three-wave mixing problem given that $V^{(3,0)} = 0$.

The classical interpretation of the loops in relations (A28) is quite transparent. The loop in (A28a) represents the beatings of the self-electromagnetic noise in the OPO with itself processed by the nonlinearity into a coherent signal. The first loop in (A28b) describes the propagation of the noise excited by an external "probe" signal, this noise being finally turned into a coherent signal by the nonlinearity. The second loop in (A28b) describes the nonlinear beatings of the self-noise with the "probe" signal. The loops in (A28c) describe nonlinear beatings of the self-noise with itself.

5. "Bare" diagrams for the degenerate OPO

The expression for the propagator can be found either by a purely classical consideration of a damped oscillator or, which is actually easier, comparing relation (A12) with standard quantum approaches to the resonator modes. Without the nonlinearity, the modes develop independently, so one has in fact two free lines: one for the fundamental and one for the subharmonic. The Fourier transform of the lines sought is

$$\left\{ \underset{m,\Omega}{\bullet\!\cdots\!\rightarrow\!\cdots\!\bullet} \right\} = \frac{1}{\Omega + i\gamma_m}, \tag{A29}$$

where the arrow shows the direction of the positive frequency ω, $\Omega = \omega - \omega_m$ is the detuning and ω_m and γ_m, $m = 1, 2$, are the modes' frequencies and widths. For negative frequencies, the free propagator can be obtained using

$$\left\{ \underset{m,\Omega}{\bullet\!\cdots\!\leftarrow\!\cdots\!\bullet} \right\} = \left\{ \underset{m,\Omega}{\bullet\!\cdots\!\rightarrow\!\cdots\!\bullet} \right\}^* = \frac{1}{\Omega - i\gamma_m}, \tag{A30}$$

which expresses the reality of $D_{\rm ret}$. The left-pointing end of the line is implied to be "earlier" and the right-pointing to be "later"; cf. (A12) (recall that the way in which the diagrams are drawn reflects their causality structure before Fourier transformation).

Relations (A16) and (A18) with $H_{\rm int}$ given by (1) yield the following set of nonzero vertices in the frequency domain: (a) the $V^{(1,2)}$-type vertices,

$$\left\{ \begin{array}{c} 1,\Omega'' \\ 1,\Omega'\ 2,\Omega \end{array} \right\} = \left\{ \begin{array}{c} 1,\Omega' \\ 2,\Omega\ 1,\Omega'' \end{array} \right\} = \left\{ \begin{array}{c} 2,\Omega \\ 1,\Omega'\ 1,\Omega'' \end{array} \right\} = \left\{ \begin{array}{c} 1,\Omega'' \\ 1,\Omega'\ 2,\Omega \end{array} \right\} = \kappa \times 2\pi\delta(\Omega' + \Omega'' - \Omega), \tag{A31}$$

and (b) the $V^{(2,1)}$-type vertices,

$$\left\{ \begin{array}{c} 1,\Omega'' \\ 2,\Omega\ 1,\Omega' \end{array} \right\} = -\left\{ \begin{array}{c} 1,\Omega'' \\ 2,\Omega\ 1,\Omega' \end{array} \right\} = i\hbar\kappa \times 2\pi\delta(\Omega' + \Omega'' - \Omega). \tag{A32}$$

Here, the thin lines denote the arguments of the vertices and the arrows correspond to the positive frequencies; cf. (A29) and (A30). In accordance with the general rule "inputs point to the left and outputs point to the right," the $V^{(1,2)}$ vertices have two arguments pointing to the left (to the past) and one to the right (to the future), and the $V^{(2,1)}$ vertices have two arguments pointing to the future and one to the past, this reflecting their interpretation as "quantum susceptibilities." In the diagrams, left-pointing ends of the lines must be fitted to the right-pointing arguments of the vertices and vice versa. Note that the observable quantum properties of the OPO are formally due to the absence of vertices of the structure $\left\{ \underset{}{\rightarrow\!\bullet\!\leftarrow} \right\}$, thus preventing any classical interpretation of the assemblage of the $V^{(2,1)}$ vertices.

The rule "complex conjugation inverts arrows" holds for vertices (A31), (A32) and thus for any graphical object as a whole. This reflects the reality of the causal diagram techniques. To avoid confusion, note once again that the arrows correspond to *frequencies*, not to detunings or causality structure of the diagrams.

As was already mentioned above, the units we use in this paper allow Planck's constant to be eliminated from all the relations which have a classical interpretation. In particular, the diagram line (A29) and the "nonlinear" vertices (A31), which are in essence classical quantities, lack Planck's constant. At the same time, it naturally turns up in the noise vertices (A32) which are inherently quantum objects.

6. Graphical equations for the degenerate OPO

Owing to the phase-definite pumping the problem is not time-uniform and Fourier transformation is thus performed independently on each argument of the graphical objects comprising a diagram. The quantities defined by (9) and (10) thus correspond to the following graphical objects in the frequency domain ($l, m = 1, 2$),

$$K_{\Omega ml} = \left\{ \underset{l,\Omega \qquad\qquad m,\Omega}{\bullet\!\rightarrow\!\cdots\!\rightarrow\!\bullet} \right\}, \quad \tilde{K}_{\Omega ml} = \left\{ \underset{l,-\Omega \qquad\qquad m,\Omega}{\bullet\!\leftarrow\!\cdots\!\rightarrow\!\bullet} \right\}, \tag{A33}$$

$$G_{\Omega ml} = \left\{ \underset{l,\Omega \qquad\qquad m,\Omega}{\searrow\!\cdots\!\swarrow} \right\}, \quad \tilde{G}_{\Omega ml} = \left\{ \underset{l,-\Omega \qquad\qquad m,\Omega}{\swarrow\!\cdots\!\searrow} \right\} \tag{A34}$$

[recall that the arrows show frequencies; cf. (A29)]. As a rule, in the case where $l = m = 1$ these indices will be

omitted.

Consider first the noise source on the subharmonic. It is convenient to return to the time representation for the diagrams. Using relation (A27) and the expression for the noise source on the fundamental in the one-loop approximation,

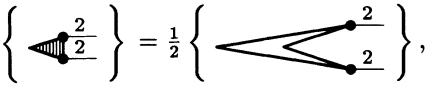

(A35)

one finds the "noise" source on the subharmonic to be

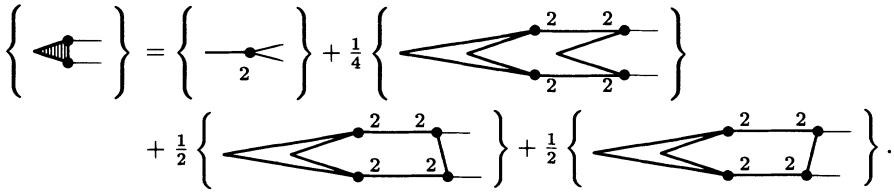

(A36)

These are the two-loop diagrams picked by the one-loop Dyson equations. It is easy to check that some of the omitted two-loop diagrams are of the same order of magnitude as the ones retained in (A36). Compare, for example, one of the diagrams in (A36),

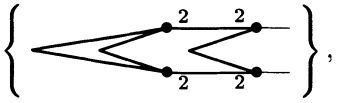

(A37)

with the following diagram omitted in the "one-loop" approximation:

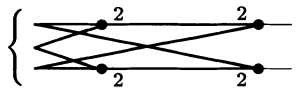

(A38)

Diagram (A38) would be small compared to (A37) if the characteristic times of the subharmonic were small compared to that of the fundamental. Not too close to the threshold, this is exactly opposite to the relation actually existing, $\gamma_2 \gg \Gamma$. In the threshold region, it is natural to expect that the characteristic times for both modes will be the same, resulting in (A37) and (A38) being of the same order of magnitude.

These considerations may be supported by directly computing diagrams (A37) and (A38). Under the approximations specified in the main body of the paper,

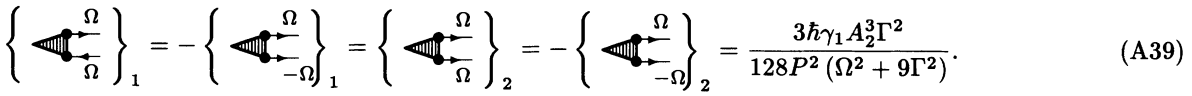

(A39)

Here, $\{\cdots\}_1$ and $\{\cdots\}_2$ correspond to the contribution of diagrams (A37) and(A38), respectively, and P is the parameter (23). This should be compared to the "linearized" noise source value $|\hbar\kappa\alpha_2| = \hbar\gamma_1 A_2$. We see that the "accounted" and "missed" contributions are just equal and must therefore be negligible for the one-loop approach to be applicable. Most importantly, their negligibility is governed by the same parameter P given by (23) that makes applicable the approach where the loops are computed with the lines taken in the linearized approximation. This shows that the accuracy of the one-loop approach to the OPO does not extend beyond this computational approximation.

One thus has to treat the one-loop diagrams as a correction to the linearized expressions and has to neglect any higher-order corrections which formally emerge. In particular, all correction terms in (A36) should be omitted, resulting in

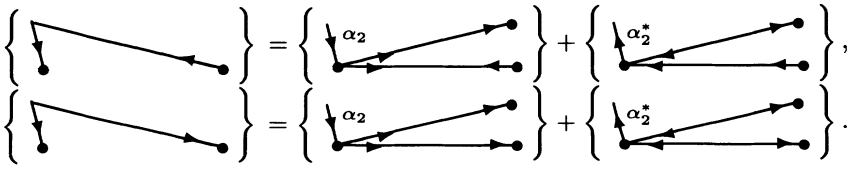

(A40a)

(A40b)

These relations are the graphical representation of Eqs. (12). They hold both in the linearized and the one-loop approximations.

If $\alpha_1 = 0$, no coherence exists between the subharmonic and fundamental, i.e., quantities (A33) and (A34) vanish if $l \neq m$. As a result, in the one-loop approximation the closed set of equations for the Fourier components of the subharmonic linear response function is found,

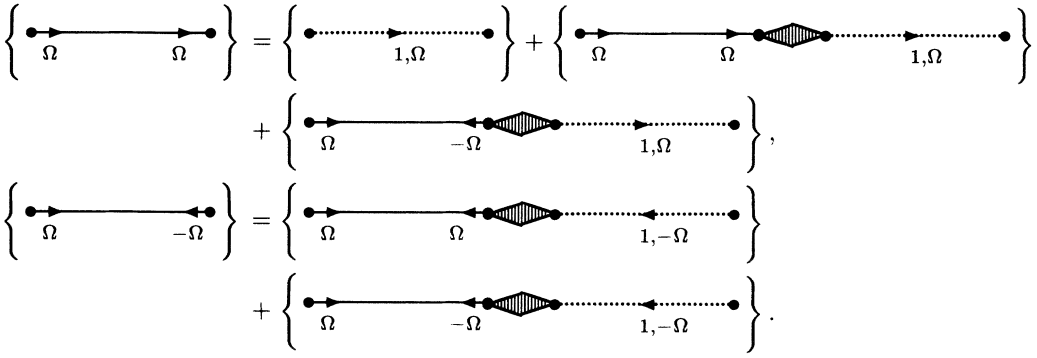

(A41a)

(A41b)

Assuming that the lines in the loops are given in the linearized approximation,

$$\left\{ \quad \right\} = \left\{ \quad \right\} = \kappa^2 \int \frac{d\Omega'}{2\pi} G_{\Omega-\Omega' 11} K_{\Omega' 22}, \tag{A42}$$

$$\left\{ \quad \right\} = \left\{ \quad \right\} = \kappa \alpha_2^*. \tag{A43}$$

In the linearized approximation, relations (A41) are found on eliminating the fundamental using relations like

$$\left\{ \quad \right\} = \left\{ \quad \right\}. \tag{A44}$$

Relations (A41) with the effective normal susceptibility

$$\left\{ \quad \right\} = \left\{ \quad \right\} = \frac{\kappa^2 |\alpha_1|^2}{\Omega + i\gamma_2} \tag{A45}$$

thus hold also in the linearized approximation.

The Dyson equation for the average field amplitude on the fundamental appears as

$$\left\{ \quad \right\} = \left\{ \quad \right\} + \left\{ \quad \right\}, \tag{A46}$$

where $\alpha_2^{(0)}$ is the "bare" field on the fundamental, i.e., the average field in the empty resonator under the same pumping conditions. Graphical notation for the average field is self-explanatory. In the linearized approximation, the medium's average polarization on the fundamental frequency is

$$\left\{ \quad \right\} = \frac{1}{2} \left\{ \quad \right\} = \frac{\kappa \alpha_1^2}{2}. \tag{A47}$$

In the one-loop approximation ($\alpha_1 = 0$) it is given by the diagram

$$\left\{ \quad \right\} = \frac{1}{2} \left\{ \quad \right\} = \frac{\kappa}{2} \int \frac{d\Omega}{2\pi} \tilde{G}_{\Omega 11}. \tag{A48}$$

For $K_{\Omega 22} \approx K_{\Omega 22}^{(0)}$, the linearized and one-loop diagram expressions formally coincide within the formal replacements

$$\left\{ \quad \right\} \Longleftrightarrow 2\pi\delta(\Omega) \left\{ \quad \right\} \times \left\{ \quad \right\}, \tag{A49a}$$

$$\left\{ \quad \right\} \Longleftrightarrow 2\pi\delta(\Omega) \left\{ \quad \right\} \times \left\{ \quad \right\}. \tag{A49b}$$

Accounting for (20), obviously this is equivalent to the replacement $\alpha_1^2 \Longleftrightarrow \hbar Q q$.

[1] See, e.g., H. J. Kimble, in *Fundamental Systems in Quantum Optics*, edited by J. Dalibard, J.-M. Raimond, and J. Zinn-Justin (Elsevier, New York, 1992), and references therein.
[2] H. R. Zaidi, Can. J. Phys. **66**, 164 (1988); **66**, 854 (1988).
[3] C. J. Mertens, T. A. B. Kennedy, and S. Swain, Phys. Rev. A **48**, 2374 (1993).
[4] R. Kubo, Rep. Prog. Phys. **XXIX**, 255 (1966).
[5] R. J. Glauber, Phys. Rev. **130**, 2529 (1963); **131**, 2766 (1963); P. L. Kelly and W. H. Kleiner, *ibid.* **136**, 316 (1964).
[6] O. V. Konstantinov and V. I. Perel, Zh. Eksp. Teor. Fiz. **39**, 197 (1961) [Sov. Phys. JETP **12**, 142 (1961)]; L. V. Keldish, *ibid.* **47**, 515 (1964) [*ibid.* **20**, 1018 (1965)].
[7] L. I. Plimak Phys. Rev. A **50**, 2120 (1994).
[8] C. W. Gardiner and M. J. Collett, Phys. Rev. A **31**, 3761 (1985); C. W. Gardiner, A. S. Parkins, and M. J. Collett, J. Opt. Soc. Am. B **B4**, 1683 (1987).
[9] D. N. Klyshko, Phys. Lett. **A137**, 334 (1989).
[10] A. N. Vassil'ev, *Functional Methods in Quantum Field Theory and Statistics* (Leningrad State University, Leningrad, 1976, in Russian); see also J. Glimm and A. Jaffe, *Quantum Physics: A Functional Integral Point of View* (Springer-Verlag, Berlin, 1981); R. J. Rivers, *Path Integral Methods in Quantum Field Theory* (Cambridge University Press, Cambridge, England, 1987).
[11] P. D. Drummond, K. J. McNeil, and D. F. Walls, Opt. Acta **28**, 211 (1981).
[12] P. Kinsler, M. Fernée, and P. D. Drummond, Phys. Rev. A **48**, 3310 (1993).
[13] L. Knöll, W. Vogel, and D.-G. Welsch, Phys. Rev. A **36**, 3801 (1987); L. Knöll and D.-G. Welsch, Prog. Quantum Electron. **16**, 135 (1992).